PCCP

PAPER

View Article Online
View Journal | View Issue

Cite this: *Phys. Chem. Chem. Phys.*, 2016, **18**, 10070

Local electric fields and molecular properties in heterogeneous environments through polarizable embedding

Nanna Holmgaard List,* Hans Jørgen Aagaard Jensen and Jacob Kongsted

Received 29th January 2016,
Accepted 23rd February 2016

DOI: 10.1039/c6cp00669h

www.rsc.org/pccp

In spectroscopies, the local field experienced by a molecule embedded in an environment will be different from the externally applied electromagnetic field, and this difference may significantly alter the response and transition properties of the molecule. The polarizable embedding (PE) model has previously been developed to model the local field contribution stemming from the direct molecule-environment coupling of the electromagnetic response properties of molecules in solution as well as in heterogeneous environments, such as proteins. Here we present an extension of this approach to address the additional effective external field effect, *i.e.*, the manifestations of the environment polarization induced by the external field, which allows for the calculation of properties defined in terms of the external field. Within a response framework, we report calculations of the one- and two-photon absorption (1PA and 2PA, respectively) properties of PRODAN–methanol clusters as well as the fluorescent protein DsRed. Our results demonstrate the necessity of accounting for both the dynamical reaction field and effective external field contributions to the local field in order to reproduce full quantum chemical reference calculations. For the lowest $\pi \rightarrow \pi^*$ transition in DsRed, inclusion of effective external field effects gives rise to a 1.9- and 3.5-fold reduction in the 1PA and 2PA cross-sections, respectively. The effective external field is, however, strongly influenced by the heterogeneity of the protein matrix, and the resulting effect can lead to either screening or enhancement depending on the nature of the transition under consideration.

1 Introduction

Local fields play a pivotal role in describing and understanding processes occurring in condensed phases and molecular environments. For instance, the highly structured arrangement of charged, polar and polarizable amino acids in a protein matrix can produce very strong local fields[1] that can be important in many aspects of protein functions, including folding, ligand–receptor specificity,[2,3] enzymatic catalytic power[4–9] and spectral tuning of the absorption properties of embedded chromophores.[1,10,11] In the presence of external electromagnetic radiation, as relevant for spectroscopies of molecules in environments, the local field acting on the embedded species is modified by the interactions involving the molecule, its environment and the external fields.[12] The environment is polarized both directly by the external field and indirectly through its interactions with the (perturbed) chromophore resulting in additional contributions to the local field. In particular, the external field is modified by these direct effects, and the effective field in the void of the chromophore, hereafter denoted as the *effective external field*, includes these modifications due to the presence of the environment. The local field effects enter into the definitions of the response and transition properties of the embedded molecule and should be properly addressed in calculations in order to obtain properties that, after orientational averaging, can be related to their experimental counterparts, being defined as the expansion coefficients between macroscopic observables and the *external* fields.

The discussion of local fields dates back to the early work by Lorentz,[13] who considered the electric field inside a fictitious spherical cavity in a dielectric continuum homogeneously polarized by an external electric field. Based on this, he derived a simple proportionality relation between the local field in the cavity and the macroscopic (*Maxwell*) field measurable in the solution bulk, which led to the definition of local field factors (tensors in general). However, the Lorentz model neglects the polarization of the medium induced by the solute molecule, which is a reasonable assumption only for non-polar molecules.[12] The Lorentz picture was later refined by Onsager to take into account the mutual interaction between the polar solute (approximated by a point dipole) and the dielectric medium.[14] Hence, Onsager represented the resulting local field as a superposition of two terms: (i) the *reaction field* representing the coupling

University of Southern Denmark, Campusvej 55, 5230 Odense M, Denmark. E-mail: nhl@sdu.dk

between the solute and the dielectric medium and (ii) the *cavity field* which is the electric field inside the empty spherical cavity due to the polarization of the dielectric induced directly by the external field, *i.e.*, the continuum counterpart of the effective external field. Accordingly, the local field tensor factorizes into a reaction field and a cavity field contribution.[15] It should be remarked that the former exists even in the absence of any applied field, while the existence of the cavity field is a manifestation of the external field.

In the framework of combined quantum–classical embedding models, which are the focus of the present work, the reaction field is self-consistently included in the determination of the wave function/density of the embedded molecule, and it therefore suffices to consider explicitly only the effective external field contribution. A component of the Onsager cavity field tensor which relates the cavity field to the *external* electric field $\mathbf{F}^{\omega}$, *i.e.*, $F_a^{\mathrm{CF},\omega} = \sum_b {}^{\mathrm{Ons}}L_{ab}^{\mathrm{E}} F_b^{\omega}$, is given by[16]

$$ {}^{\mathrm{Ons}}L_{ab}^{\mathrm{E},\omega} = \frac{3}{2\xi+1}\delta_{ab}, \quad \xi = \begin{cases} \varepsilon & \omega = 0 \\ n^2 & \omega > 0 \end{cases} \tag{1} $$

where Roman subscripts denote the Cartesian directions. $\xi \geq 1$ is the frequency-dependent dielectric permittivity of the medium describing the dielectric screening of the external electric field in the bulk solvent (the Maxwell field), ε is the static dielectric constant and n is the frequency-dependent refractive index, giving the optical dielectric constant. On the other hand, the tensor relating the cavity field to the electric Maxwell field, as in the original work, can be written as[12]

$$ {}^{\mathrm{Ons}}L_{ab}^{\mathrm{M},\omega} = \frac{3\xi}{2\xi+1}\delta_{ab} = \xi \cdot {}^{\mathrm{Ons}}L_{ab}^{\mathrm{E},\omega}. \tag{2} $$

For a spherical cavity, the cavity field will thus always be larger than the Maxwell field in the dielectric far from the cavity but screened with respect to the external field. The cavity field factor defined in eqn (2) as well as its generalization to elliptical cavities[12] has been used for many years as a correction factor for spectroscopies of solvated molecules, often in the lack of better values (see, *e.g.*, ref. 17). To allow for a more realistic representation of solute–solvent systems with molecular-shaped cavities, cavity field effects have been introduced in the framework of the polarizable continuum model (PCM)[18,19] in terms of an additional apparent surface charge distribution entering the solute Hamiltonian.[20] The rigorous derivation of this formulation was recently presented in ref. 21, and the elaborated model has been successfully applied to study various spectroscopic[22–31] and molecular response properties[32–34] of solvated systems.

In this work, we consider local fields within the polarizable embedding (PE) model,[35,36] which is a discrete quantum-classical embedding scheme designed for reliable and efficient modeling of electronic excitations as well as general electromagnetic response properties of molecules embedded in solvents and, in particular, heterogeneous environments. In the PE model, the permanent charge distribution of the fragments constituting the classically treated environment is represented by distributed permanent multipole moments usually taken at the atomic centers in the environment. In addition, the induced charge distribution of the environment is described by assigning distributed anisotropic electronic dipole–dipole polarizabilities to each site in the environment giving rise to induced dipole moments.

The PE model has, in the past few years, been elaborated to model the reaction field contribution to the molecular properties of an embedded chromophore (see, *e.g.*, ref. 35 and 37). Following the lines of ref. 38, we here extend the formulation of molecular properties in the discrete PE framework to account for effective external field effects, *i.e.*, the implications of the difference between the effective external field at the location of the quantum region and the applied field, in heterogeneous environments. Our focus is on modeling these effects on one- and two-photon absorption properties (1PA and 2PA, respectively) of an embedded chromophore. As such, we will be concerned with external optical fields in the UV-vis region, for which the nuclear translations and rotations cannot follow and the response of the system to the external field therefore only involves the electronic degrees of freedom. To demonstrate the performance of the proposed extension of the model, we present two test applications. First, we compare the PE results for small solute–solvent clusters to full quantum mechanical (QM) reference calculations and show that the inclusion of the effective external field significantly improves the absolute cross sections obtained within the PE framework. Second, we apply the extended model to study local field effects in a protein environment and investigate how the heterogeneity of the protein affects the effective external field effects.

The remainder of this work is organized as follows. Section 2 gives an outline of the PE model and presents our extension to describe electromagnetic molecular response properties including effective external field effects. Computational details are given in Section 3, and the 1PA and 2PA results obtained within the presented model are discussed in Section 4. Finally, concluding remarks are given in Section 5.

2 Theory

In this section, we outline the PE model and present the proposed extension to describe local field effects on the absorption properties of embedded systems including the effective external field contribution. Although we here provide the expressions within a variational framework, the discussion of local fields is general, irrespective of the level of theory applied in the quantum region. Details concerning derivations of the PE environmental terms for the wave function optimization and the reaction field contributions to response properties can be found, *e.g.*, in ref. 35 for Hartree–Fock and Kohn–Sham density functional theory (KS-DFT) (collectively referred to as SCF) up to quadratic response theory, in ref. 37 for multi-configurational self-consistent-field theory up to linear response theory, and in ref. 39 for coupled cluster theory up to quadratic response. We use $|0\rangle$ to denote a variationally optimized reference state of the quantum region, and $|\tilde{0}\rangle$ to

represent the corresponding time-dependent state. For simplicity, the explicit response expressions will be given for an SCF parameterization. Atomic units will be used throughout, unless stated otherwise.

2.1 Outline of the polarizable embedding model

In the PE model, the energy functional for a composite system, consisting of a quantum region embedded in a polarizable environment (also referred to as the PE region), is partitioned into three contributions

$$\mathcal{E}_{\mathrm{PEQM}} = \mathcal{E}_{\mathrm{QM}} + \mathcal{E}_{\mathrm{PE}} + \mathcal{E}_{\mathrm{int}}, \tag{3}$$

where $\mathcal{E}_{\mathrm{QM}}$ is the energy of the quantum region (including wave function polarization); and $\mathcal{E}_{\mathrm{PE}}$ is the internal energy of all fragments in the PE region, including the electrostatic interaction between these fragments, but excluding the energy associated with the creation of the dipole polarization in the environment. The latter contributes to the variational optimization of the energy, and it is therefore convenient to include the polarization energy of the PE region in $\mathcal{E}_{\mathrm{int}}$ together with the contributions arising from the direct interactions of the quantum region with the environment. The interaction energy can be decomposed as

$$\mathcal{E}_{\mathrm{int}} = \mathcal{E}_{\mathrm{es}} + \mathcal{E}_{\mathrm{ind}} + \mathcal{E}_{\mathrm{disp\text{-}rep}}, \tag{4}$$

where $\mathcal{E}_{\mathrm{es}}$ and $\mathcal{E}_{\mathrm{ind}}$ are the electrostatic contributions arising from interactions between the quantum region and the permanent and induced charge distributions of the environment, respectively. $\mathcal{E}_{\mathrm{disp\text{-}rep}}$ collects the energy terms related to dispersion and exchange-repulsion effects. These are typically treated only at the energy level using a Lennard-Jones (LJ) potential,[40] which does not affect the electronic properties associated with the quantum region of the system. This term is therefore not included in the response treatment described in Section 2.3.

The $\mathcal{E}_{\mathrm{es}}$ term accounts for the interactions between the permanent multipole moments in the environment and the electrons and nuclei in the quantum region. By adopting a multi-index notation,[41] $\mathcal{E}_{\mathrm{es}}$ can be written as[42]

$$\begin{aligned}\mathcal{E}_{\mathrm{es}} &= \mathcal{E}_{\mathrm{mul,e}} + \mathcal{E}_{\mathrm{mul,n}} \\ &= \langle 0|\hat{v}^{\mathrm{es}}|0\rangle + \sum_{s=1}^{S}\sum_{|k|=0}^{K_s}\frac{(-1)^{|k|}}{k!}M_s^{(k)}\sum_{m\in\mathrm{QM}}T_{sm}^{(k)}Z_m,\end{aligned} \tag{5}$$

where the norm and factorial of a multi-index $k = (k_x,k_y,k_z)$ are defined as $|k| = k_x + k_y + k_z$ and $k! = k_x!k_y!k_z!$, respectively. The $|k|$ summation runs over the $(|k| + 1)(|k| + 2)/2$ multi-indices for a given $|k|$, *e.g.*, for $|k| = 1$, the summation is over the three Cartesian components (1,0,0), (0,1,0) and (0,0,1) defining the components of a dipole moment. S is the number of sites in the PE region. Within a second quantization formalism, the electrostatic operator $\hat{v}^{\mathrm{es}}$ is defined as

$$\hat{v}^{\mathrm{es}} = \sum_{s=1}^{S}\sum_{|k|=0}^{K_s}\frac{(-1)^{|k|}}{k!}M_s^{(k)}\sum_{pq\in\mathrm{QM}}t_{s,pq}^{(k)}\hat{E}_{pq}, \tag{6}$$

where $\hat{E}_{pq}$ is a one-electron orbital excitation operator[43] and p and q label general molecular orbital indices belonging to the quantum region. $M_s^{(k)}$ is a Cartesian component of the $|k|$'th-order multipole moment located at the s'th site in the environment, and Z_m is the nuclear charge of the m'th nucleus in the quantum region. K_s is the truncation level of the multipole expansion assigned to the s'th site. The $t_{s,pq}^{(k)}$ integrals are given by

$$t_{s,pq}^{(k)} = -\langle\phi_p(\mathbf{r}_i)|T_{si}^{(k)}|\phi_q(\mathbf{r}_i)\rangle, \tag{7}$$

and involves the k'th component of the $|k|$'th-order interaction tensor defined as a $|k|$'th-order derivative of the potential between two sites i and j, *i.e.*,

$$T_{ij}^{(k)} = \frac{\partial^{|k|}}{\partial x_j^{k_x}\partial y_j^{k_y}\partial z_j^{k_z}}\left(\frac{1}{|\mathbf{r}_j - \mathbf{r}_i|}\right). \tag{8}$$

For a linearly responsive environment, the variationally optimized induction energy due to polarization of the environment both internally and by the electrons and nuclei in the quantum region amounts to half the corresponding interaction energy[44–46]

$$\mathcal{E}_{\mathrm{ind}} = -\frac{1}{2}\left[\boldsymbol{\mu}^{\mathrm{ind}}\left(\mathbf{F}^{\mathrm{tot}}\right)\right]^{\mathrm{T}}\mathbf{F}^{\mathrm{tot}}. \tag{9}$$

Here, $\boldsymbol{\mu}^{\mathrm{ind}}$ is a $3S$-dimensional column vector holding the induced dipole moments produced by the electric field acting on the environmental sites

$$\mathbf{F}^{\mathrm{tot}} = \mathbf{F}^{\mathrm{mul}} + \langle 0|\hat{\mathbf{F}}^{\mathrm{e}}|0\rangle + \mathbf{F}^{\mathrm{n}}, \tag{10}$$

where $\mathbf{F}^{\mathrm{mul}}$, $\langle 0|\hat{\mathbf{F}}^{\mathrm{e}}|0\rangle$ and $\mathbf{F}^{\mathrm{n}}$ are the $3S$-dimensional electric field vectors arising from the permanent multipoles in the environment as well as from the electrons and nuclei in the quantum region, respectively. Superscript T denotes transposition.

The induced dipole moments are obtained as the classical linear response to the electric field

$$\boldsymbol{\mu}^{\mathrm{ind}}\left(\mathbf{F}^{\mathrm{tot}}\right) = \mathbf{K}\mathbf{F}^{\mathrm{tot}}, \tag{11}$$

where $\mathbf{K}$ is the $(3S \times 3S)$-dimensional classical linear response matrix given by[47]

$$\mathbf{K} = \begin{pmatrix} \boldsymbol{\alpha}_1^{-1} & -\mathbf{T}_{12}^{(2)} & \cdots & -\mathbf{T}_{1S}^{(2)} \\ -\mathbf{T}_{21}^{(2)} & \boldsymbol{\alpha}_2^{-1} & \ddots & \vdots \\ \vdots & \ddots & \ddots & -\mathbf{T}_{(S-1)S}^{(2)} \\ -\mathbf{T}_{S1}^{(2)} & \cdots & -\mathbf{T}_{S(S-1)}^{(2)} & \boldsymbol{\alpha}_S^{-1} \end{pmatrix}^{-1}. \tag{12}$$

This matrix holds the inverse of the distributed electric dipole–dipole polarizability tensors on the diagonal, and second-order interaction tensors in the off-diagonal blocks.

The wave function/density describing the quantum region is determined by requiring $\mathcal{E}_{\mathrm{PEQM}}$ to be stationary with respect to the wave function/density of the quantum region. The only difference in the resulting wave function optimization

equations compared to the vacuum counterparts is the presence of the PE embedding operator

$$\hat{v}^0_{\mathrm{PE}} = \hat{v}^{\mathrm{es}} + \hat{v}^{\mathrm{ind}}, \tag{13}$$

where the induction part reads as

$$\hat{v}^{\mathrm{ind}} = -\sum_{s=1}^{S} \left[\boldsymbol{\mu}^{\mathrm{ind}}_s\left(\mathbf{F}^{\mathrm{tot}}\right)\right]^{\mathrm{T}} \hat{\mathbf{F}}^{\mathrm{e}}_s; \quad \hat{\mathbf{F}}^{\mathrm{e}}_s = -\sum_{pq\in \mathrm{QM}} \boldsymbol{t}^{(1)}_{s,pq} \hat{E}_{pq}. \tag{14}$$

Having defined the basics of the PE model as well as the PE embedding operator relevant for optimization of the ground state wave function, we move to consider the molecular response of the composite system to external electric fields with particular emphasis on 1PA and 2PA properties. Before proceeding to the property expressions in Section 2.3, we explicate the division of the local field in the PE model into reaction field and effective external field contributions.

2.2 The local field in the quantum region

In the PE model, the local electric field (excluding the internal field from the quantum region itself) at location $\mathbf{R}_n$ within the quantum region is the sum of the external field and the fields produced by the permanent and induced charge distribution of the environment

$$F^{\mathrm{LF}}_a(\mathbf{R}_n) = F^t_a(\mathbf{R}_n) + F^{\mathrm{mul}}_a(\mathbf{R}_n) + \sum_{s=1}^{S}\sum_b T^{(2)}_{sn,ab}\mu^{\mathrm{ind}}_{s,b}\left(\tilde{\mathbf{F}}^{\mathrm{tot}}\right). \tag{15}$$

In the long wavelength limit, the external field is uniform across the dimension of the system, $F^t_a(\mathbf{R}_n) = F^t_a$, and can be written in the form

$$F^t_a = \sum_k \mathrm{e}^{-i\omega_k t} F^{\omega_k}_a, \tag{16}$$

where the summation runs over both positive and negative indices. ω_k is the angular frequency, $\omega_{-k} = -\omega_k$, and $F^{\omega_k}_a = \left[F^{-\omega_k}_a\right]^*$ is the Fourier amplitude. The field vector generating the induced dipoles in eqn (15) is the time-dependent analogue of eqn (10) augmented with the time-dependent external field, *i.e.*,

$$\tilde{\mathbf{F}}^{\mathrm{tot}} = \mathbf{F}^{\mathrm{mul}} + \mathbf{F}^{\mathrm{n}} + \left\langle\tilde{0}\middle|\hat{\mathbf{F}}^{\mathrm{e}}\middle|\tilde{0}\right\rangle + \mathbf{F}^t. \tag{17}$$

As discussed in the Introduction, the local field in a continuum solvation approximation consists of a reaction field and the effective external field (cavity field). In the PE model, the reaction field originates from the dipole polarization in eqn (15) induced by the second and third terms of eqn (17), while the dipole polarization due to the last term in eqn (17) gives rise to the effective external field effect. It is common to distinguish between static and dynamic reaction field contributions: the former is the field generated by the dipole polarization in the environment reflecting the static density of the quantum region, while the latter stems from the environment polarization induced by the oscillating density of the quantum region (at frequency ω_k) due to the time-dependent external field. An additional term to the local field arises in the PE model due to the permanent multipole moments of the environment. As will be outlined in Section 2.3, the effects of this term along with those of the reaction field are self-consistently included in the optimization of the wave function of the quantum region. We will therefore only consider the effective external field effects explicitly in the following.

In the discrete PE framework, the part of eqn (15) defining the effective external field in the quantum region is the sum of the external field and the field due to the dipole moments induced by the direct interaction between the polarizable sites in the environment and the external field. For a linearly responsive environment, a Fourier amplitude of the effective external field can be written as

$$F^{\mathrm{EEF},\omega_k}_a(\mathbf{R}_n) = F^{\omega_k}_a + \sum_{s=1}^{S}\sum_b T^{(2)}_{sn,ab}\mu^{\mathrm{ind}}_{s,b}(\mathbf{F}^{\omega_k}). \tag{18}$$

Along the lines of ref. 48, the modification of the external field due to the influence of the surrounding environment may conveniently be expressed in terms of effective external field tensors defined as

$$L^{\omega_k}_{ab}(\mathbf{R}_n) = \frac{\partial F^{\mathrm{EEF},\omega_k}_a(\mathbf{R}_n)}{\partial F^{\omega_k}_b} = \delta_{ab} + \sum_{s=1}^{S}\sum_c T^{(2)}_{sn,ac}\frac{\partial \mu^{\mathrm{ind}}_{s,c}(\mathbf{F}^{\omega_k})}{\partial F^{\omega_k}_b}. \tag{19}$$

It will be shown below that, the implications of effective external field effects on the molecular properties can be approximated by inclusion of such effective external field tensors.

2.3 Response theory in a molecular environment

In this section, we illustrate how the local field, and in particular the effective external field contribution, influences the 1PA and 2PA properties of a transition localized in the quantum region of a composite system. Accordingly, we focus on the linear and quadratic response functions of the composite system with respect to a uniform oscillating electric field. The time-dependent perturbation operator therefore becomes

$$\hat{V}^t = \sum_k \mathrm{e}^{-i\omega_k t}\sum_a \hat{V}^{\omega_k}_a F^{\omega_k}_a, \tag{20}$$

where $\hat{V}^{\omega}_a = -\hat{\mu}_a$ is minus the a'th component of the electric dipole operator.

To derive the molecular response properties, we follow the Fourier component variational perturbation theory approach (ref. 49), where the ground-state energy is replaced with the more general time-averaged quasi-energy $\{Q_{\mathrm{PEQM}}(t)\}_T$. By analogy with the time-independent case, molecular response functions can accordingly be defined as derivatives of $\{Q_{\mathrm{PEQM}}(t)\}_T$ with respect to the field amplitudes of the external field. As will become clear below [eqn (24) and (25)] this leads to response functions that are symmetric with respect to the operators involved, as appropriate for the description of transition properties. Note that an alternative formulation follows from the Ehrenfest approach in which the electric properties are defined from a perturbation expansion of the expectation value of the electric dipole operator. In this case emphasis is on the quantum region and the resulting response functions will take on asymmetric forms accordingly.

The time-dependent quasi-energy functional for the composite system is obtained by adding $\mathcal{E}_{\mathrm{PE}}{}'$ and $\mathcal{E}_{\mathrm{int}}{}'$ (omitting the

constant $\mathcal{E}_{\text{disp-rep}}$ term) to the vacuum quasi-energy $Q_{\text{QM}}(t)$ of the quantum region

$$Q_{\text{PEQM}}(t) = Q_{\text{QM}}(t) + \langle\tilde{0}|\hat{v}^{\text{es}}|\tilde{0}\rangle - \frac{1}{2}\left[\boldsymbol{\mu}^{\text{ind}}\left(\tilde{\mathbf{F}}^{\text{tot}}\right)\right]^{\text{T}}\tilde{\mathbf{F}}^{\text{tot}} + \mathcal{E}_{\text{PE}}{}', \tag{21}$$

where an apostrophe is used to signify the inclusion of interaction terms with the external field. The response functions and equations are then determined by decomposing $Q_{\text{PEQM}}(t)$ into Fourier components, performing a time-averaging and using the Fourier component variational perturbation theory approach. In particular, after applying Wigner's $2n + 1$ rule[50] and differentiation with respect to the external field amplitudes, we obtain the linear

$$\frac{\mathrm{d}^2\left\{^{2n+1}Q^{(2)}_{\text{PEQM}}(t)\right\}_T}{\mathrm{d}F_a^{-\omega}\mathrm{d}F_b^{\omega}} = -\left[\bar{\alpha}_{ab}(-\omega;\omega) + \alpha^{\text{PE}}_{ab}(-\omega;\omega)\right], \tag{22}$$

and the quadratic response function

$$\frac{\mathrm{d}^3\left\{^{2n+1}Q^{(3)}_{\text{PEQM}}(t)\right\}_T}{\mathrm{d}F_a^{-\omega_\sigma}\mathrm{d}F_b^{\omega_1}\mathrm{d}F_c^{\omega_2}} = \bar{\beta}_{abc}(-\omega_\sigma;\omega_1,\omega_2) + \bar{\beta}^{\text{PE}}_{abc}(-\omega_\sigma;\omega_1,\omega_2), \tag{23}$$

of the composite system, where $\omega_\sigma = (\omega_1 + \omega_2)$. $\boldsymbol{\alpha}^{\text{PE}}$ and $\boldsymbol{\beta}^{\text{PE}}$ are the explicit environment contributions to the linear polarizability and first hyperpolarizability, respectively, of the composite system, whereas $\bar{\boldsymbol{\alpha}}$ and $\bar{\boldsymbol{\beta}}$ are the effective properties of the embedded quantum region involving the interactions with the environment. Note that due to the use of gas-phase expansion points for the distributed properties of the environment in the PE model, $\boldsymbol{\alpha}^{\text{PE}}$ and $\boldsymbol{\beta}^{\text{PE}}$ model the molecular polarizabilities of the environment in the absence of the quantum region.[47] Hyperpolarizabilities in the environment are neglected (*i.e.*, $\boldsymbol{\beta}^{\text{PE}} = \mathbf{0}$, which anyway vanishes for isotropic systems) in the current version of the PE model, and the polarizabilites are approximated with their static limit for all frequencies. This is a reasonable approximation for frequencies in the UV-vis region that are far from resonances in the environment.

The effective properties are given by

$$\bar{\alpha}_{ab}(-\omega;\omega) = -\left\langle\left\langle \hat{\bar{V}}_a^{-\omega};\hat{\bar{V}}_b^{\omega}\right\rangle\right\rangle = \bar{\mathbf{V}}_a^{\omega[1]\dagger}\bar{\mathbf{x}}_b^{\omega}, \tag{24}$$

$$\begin{aligned}\bar{\beta}_{abc}(-\omega_\sigma;\omega_1,\omega_2) &= \left\langle\left\langle \hat{\bar{V}}_a^{-\omega_\sigma};\hat{\bar{V}}_b^{\omega_1},\hat{\bar{V}}_c^{\omega_2}\right\rangle\right\rangle \\ &= \bar{\mathbf{V}}_a^{-\omega_\sigma[2]}\bar{\mathbf{x}}_b^{\omega_1}\bar{\mathbf{x}}_c^{\omega_2} + \bar{\mathbf{V}}_b^{\omega_1[2]}\bar{\mathbf{x}}_a^{-\omega_\sigma}\bar{\mathbf{x}}_c^{\omega_2} + \bar{\mathbf{V}}_c^{\omega_2[2]}\bar{\mathbf{x}}_a^{-\omega_\sigma}\bar{\mathbf{x}}_b^{\omega_1} \\ &\quad + \mathcal{P}_{abc}\left(\mathbf{E}^{[3]} + \omega_\sigma\mathbf{S}^{[3]}\right)\bar{\mathbf{x}}_a^{-\omega_\sigma}\bar{\mathbf{x}}_b^{\omega_1}\bar{\mathbf{x}}_c^{\omega_2},\end{aligned} \tag{25}$$

where $\mathcal{P}_{abc}$ averages over all possible permutations of the $(a, -\sigma)$, $(b, 1)$ and $(c, 2)$ joint dipole operator-frequency indices. The response quantities appearing in eqn (24) and (25) are defined in Table 1 for an SCF parameterization, and the first-order response vectors (*e.g.*, $\bar{\mathbf{x}}_b^{\omega_1}$) are found by solving the linear response equations

$$\bar{\mathbf{x}}_b^{\omega_1} = \left[\mathbf{E}^{[2]} - \omega_1\mathbf{S}^{[2]}\right]^{-1}\bar{\mathbf{V}}_b^{\omega_1[1]}. \tag{26}$$

The elements of the electronic Hessian $\mathbf{E}^{[2]}$ and metric matrix $\mathbf{S}^{[2]}$ are ordered in the usual way with excitations before de-excitations in columns and opposite in rows.[51]

The static reaction field contribution enters through $\hat{v}^0_{\text{PE}}$ in eqn (13), while the direct and indirect responses of the environment to the external field lead to contributions that can conveniently be represented by introducing two additional PE operators

$$\hat{v}^b_{\text{PE}}(\omega) = -\sum_{s=1}^{S}\frac{\partial\left[\boldsymbol{\mu}^{\text{ind}}_s(\mathbf{F}^{\omega})\right]^{\text{T}}}{\partial F_b^{\omega}}\hat{\mathbf{F}}^{\text{e}}_s, \tag{27}$$

$$\hat{v}^{q_i}_{\text{PE}} = -\sum_{s,s'=1}^{S}\left\langle 0\left|\left[\hat{\mathbf{F}}^{\text{e}}_s,\hat{q}_i\right]\right|0\right\rangle^{\text{T}}\mathbf{K}_{ss'}\hat{\mathbf{F}}^{\text{e}}_{s'}. \tag{28}$$

The latter term is mediated by the external field-induced changes in the quantum region and as such represents the effect of the dynamical reaction field. As shown in Table 1, this term, together with the static contributions from the environment,

Table 1 Vectors and matrices used in PE–SCF linear and quadratic response theory. The PE response operators $\hat{v}^b_{\text{PE}}(\omega)$ and $\hat{v}^{q_i}_{\text{PE}}$ are defined in eqn (27) and (28), respectively, and $\hat{v}^0_{\text{PE}}$ is given in eqn (13). $\hat{q}_i$ denotes excitation ($i > 0$) and de-excitation ($i < 0$) operators

		PE contributions[a]	
Quantity	Vacuum contributions	Static	Dynamic
$E^{[2]}_{ij}$	$\langle 0\|[\hat{q}_i,[\hat{H}_{\text{QM}},\hat{q}_j]]\|0\rangle$	$\langle 0\|[\hat{q}_i,[\hat{v}^0_{\text{PE}},\hat{q}_j]]\|0\rangle$	$\left\langle 0\left\|\left[\hat{q}_i,\hat{v}^{q_j}_{\text{PE}}\right]\right|0\right\rangle$
$S^{[2]}_{ij}$	$\langle 0\|[\hat{q}_i,\hat{q}_j]\|0\rangle$	—	—
$\bar{V}^{\omega[1]}_{b,i}$	$\langle 0\|[\hat{q}_i,\hat{v}_b{}^{\omega}]\|0\rangle$	—	$\langle 0\|[\hat{q}_i,\hat{v}^b_{\text{PE}}(\omega)]\|0\rangle$
$E^{[3]}_{ijk}$	$\frac{1}{6}\left\langle 0\left\|\left[\left[\left[\hat{H}_{\text{QM}},\hat{q}_i\right],\hat{q}_j\right],\hat{q}_k\right]\right|0\right\rangle$	$\frac{1}{6}\left\langle 0\left\|\left[\left[\left[\hat{v}^0_{\text{PE}},\hat{q}_i\right],\hat{q}_j\right],\hat{q}_k\right]\right|0\right\rangle$	$\frac{1}{2}P^{ijk}\left\langle 0\left\|\left[\left[\hat{v}^{q_i}_{\text{PE}},\hat{q}_j\right],\hat{q}_k\right]\right|0\right\rangle$
$S^{[3]}_{ijk}$	$\frac{1}{6}\left\langle 0\left\|\left[\left[\hat{q}_i,\hat{q}_j\right],\hat{q}_k\right]\right|0\right\rangle$	—	—
$\bar{V}^{\omega[2]}_{b,ij}$	$\frac{1}{2}P^{ij}\left\langle 0\left\|\left[\left[\hat{V}^{\omega}_b,\hat{q}_i\right],\hat{q}_j\right]\right|0\right\rangle$	—	$\frac{1}{2}P^{ij}\left\langle 0\left\|\left[\left[\hat{v}^b_{\text{PE}}(\omega),\hat{q}_i\right],\hat{q}_j\right]\right|0\right\rangle$

[a] $P^{ij\cdots}$ operator generates the sum over all possible permutations of the $ij\cdots$ operator indices.

enters the electronic Hessian and higher-order analogues. The effective external field is a consequence of the direct environmental response to the external field, and it is manifested in an explicit environment term to the property derivatives. Concretely, the perturbation operator from the external field is augmented by $\hat{v}^b_{\mathrm{PE}}(\omega)$ [eqn (27)], and the resulting effective perturbation operator becomes

$$\hat{\bar{V}}^{\omega}_b = \hat{V}^{\omega}_b + \hat{v}^b_{\mathrm{PE}}(\omega), \tag{29}$$

where the last term represents the field from the dipole polarization of the environment induced by the external field.

As noted above, molecular properties are directly associated with the response functions. In particular, excitation energies and 1PA (2PA) transition moments can be found from a pole and residue analysis of the linear (quadratic) response function. The poles of the linear response function in eqn (22) associated with excitations in the quantum region are dictated by the first term $\bar{\boldsymbol{\alpha}}(-\omega;\omega)$, while the second term, the PE environment contribution, has no effect on excitation energies in the quantum region. Hence, the excitation energies are found by solving the generalized eigenvalue equation

$$(\mathbf{E}^{[2]} - \omega_{k0}\mathbf{S}^{[2]})\mathbf{x}_k = \mathbf{0}, \tag{30}$$

where $\mathbf{x}_k$ represents the k'th excited state with excitation energy ω_{k0}. The associated 1PA strengths can be determined as single residues of the first term in eqn (24)

$$\lim_{\omega\to\omega_{k0}}(\omega-\omega_{k0})\left\langle\left\langle \hat{\bar{V}}^{-\omega}_a;\hat{\bar{V}}^{\omega}_b\right\rangle\right\rangle = \bar{\mathbf{V}}^{\omega_{k0}[1]\dagger}_a\mathbf{x}_k\mathbf{x}_k^{\dagger}\bar{\mathbf{V}}^{\omega_{k0}[1]}_b. \tag{31}$$

The 2PA strength is formally related to the single residue of the cubic response function,[52] however, the components of the underlying 2PA transition matrix, $\bar{S}^{k0}_{ab}$, can be extracted from the single residue of the quadratic response function as

$$\begin{aligned}\bar{S}^{k0}_{ab} &= \bar{\mathbf{V}}^{-\omega[2]}_a\bar{\mathbf{x}}^{\omega}_b\mathbf{x}_k + \bar{\mathbf{V}}^{\omega[2]}_b\bar{\mathbf{x}}^{-\omega}_a\mathbf{x}_k \\ &\quad + \mathcal{P}_{ab}\left(\mathbf{E}^{[3]} - \omega\mathbf{S}^{[3]}\right)\bar{\mathbf{x}}^{-\omega}_a\bar{\mathbf{x}}^{\omega}_b\mathbf{x}_k; \quad \omega = -\omega_{k0}/2.\end{aligned} \tag{32}$$

We next consider the relation between the effective external field corrected absorption properties and the effective external field tensor defined in eqn (19). Recasting the transition electric field in the environmental term in $\bar{\mathbf{V}}^{\omega}_a$ to a dipolar form ($\mathbf{R}$ denotes an expansion point within the quantum region) the property derivative matrices including effective external field effects can be related to those without (the unbarred property derivatives, *e.g.*, $\mathbf{V}^{\omega[1]}_a$) in the following way

$$\bar{\mathbf{V}}^{\omega[1]}_b = \sum_a \mathbf{V}^{\omega[1]}_a L^{\omega}_{ab}(\mathbf{R}); \quad \bar{\mathbf{V}}^{\omega[2]}_b = \sum_a \mathbf{V}^{\omega[2]}_a L^{\omega}_{ab}(\mathbf{R}). \tag{33}$$

Note that the Taylor expansion implied in eqn (33) introduces an arbitrariness due to the choice of expansion point. Combining eqn (31)–(33), it is found that when a one-center transition point-dipole field provides a reasonable description of the non-expanded transition electric field, the transition moments including effective external field effects can be estimated from matrix(-vector) products between the transition moments excluding the modification of the external field and the effective external field tensor.

3 Computational details

To study the influence of local field effects, and the effective external field contribution in particular, we consider the 1PA and 2PA properties of two systems: (i) cluster models for four statistically independent configurations of PRODAN (6-propionyl-2-dimethylaminonaphthalene) solvated in methanol (MeOH), including solvent molecules having at least one atom within 3 Å of the solute and (ii) a monomer of the red fluorescent protein, DsRed.[53]

The structures of the PRODAN–MeOH clusters were taken from a 10 ns classical molecular dynamics (MD) trajectory. Before extracting the solute–solvent clusters, the solute geometries were optimized at the B3LYP[54–57]/6-311++G**[58,59] level of theory in the presence of the fixed MeOH molecules described using the PE model.[40] The embedding potential representing the solvent molecules consisted of atom-centered permanent electric multipole moments up to and including quadrupoles and anisotropic electric dipole–dipole polarizabilities. LJ parameters for PRODAN were taken from ref. 60, while Amber[61] LJ parameters were used for the solvent. The embedding parameters were computed at the CAM-B3LYP[62]/aug-cc-pVDZ[63,64] level of theory according to the localized property (LoProp[65]) approach. Unperturbed and first-order perturbed density matrices were generated using the Dalton program[66,67] from which the distributed multipole moments and polarizabilities were subsequently obtained using the Loprop-for-Dalton Python script.[68] The basis set was recontracted to an atomic natural orbital type basis as required for the LoProp approach.[65]

The structure of a monomer of the DsRed protein was taken from ref. 69, where chain A of the crystal structure (PDB ID: 1ZGO[70]) was refined using an electrostatic embedding quantum mechanics/molecular mechanics scheme. For the property calculations, the quantum region consists of the chromophore together with residues 65–68 as well as the N and HN atoms of Gln64 and Ser69, appropriately capped with hydrogen link atoms. The remainder of the protein was represented by a LoProp derived embedding potential computed at the B3LYP/6-31+G*[58,59,71–73] level of theory, adopting the fragmentation strategy in ref. 74. Thole's damping scheme[75] was adopted for the interactions between induced dipole moments in the PE region to avoid overpolarization of close-lying sites in the property calculations. Charges within 1.3 Å of the quantum region were relocated to the two nearest atoms in the PE region, whereas higher-order multipoles and polarizabilities within this range were removed.

The 1PA and 2PA properties of the lowest $\pi \rightarrow \pi^*$ transition of both PRODAN in MeOH and DsRed were computed using the PE model by employing the CAM-B3LYP functional and the aug-cc-pVDZ and the 6-31+G* basis set, respectively. The same level of QM theory was employed in the full QM reference

calculations on cluster models. In particular, the use of the long-range-corrected CAM-B3LYP functional improves the well-known issues of standard exchange–correlation functionals used in KS-DFT in treating extended systems and charge-transfer excited states.[76,77] All 1PA and 2PA calculations were performed in a development version of the Dalton program. The PE contributions were handled by the PE library,[42,78] which has been interfaced with Dalton. The generation of the embedding potentials was facilitated by the PE Assistant Script.[42] The conversion of microscopic 2PA transition probabilities (defined by eqn (3) and (4) in ref. 79) to macroscopic cross sections was done using eqn (1) in ref. 79 with $N = 4$ and a half width at half maximum of 0.1 eV using a Lorentzian broadening. This is consistent with the procedure used in our previous work on DsRed.[69]

4 Results and discussion

In this section, we present and discuss the results of the PE-DFT calculations obtained with (PE-EEF) and without (PE) inclusion of the effective external field. We recall that, in the discrete PE model, the account of the effective external field effect leads to properties that are defined with respect to the external electric field. In particular, this allows for a direct comparison of PE-EEF absorption cross sections to full QM reference results.

4.1 PRODAN in methanol

Before applying the presented PE extension to larger systems, we validate the effective external field corrected PE model on absorption cross sections of a small solute–solvent cluster by comparing with the corresponding supermolecular TD-DFT calculations (denoted as QM). In this comparison, it should be kept in mind that intermolecular non-electrostatic effects are accounted for only (within a CAM-B3LYP framework) in the latter, and thus, a complete agreement cannot be expected. We consider the 1PA and 2PA cross sections of the intramolecular charge-transfer $\pi \rightarrow \pi^*$ transition in the polarity-sensitive probe PRODAN solvated in water, including solvent molecules within 3 Å of the solute (see Fig. 1).

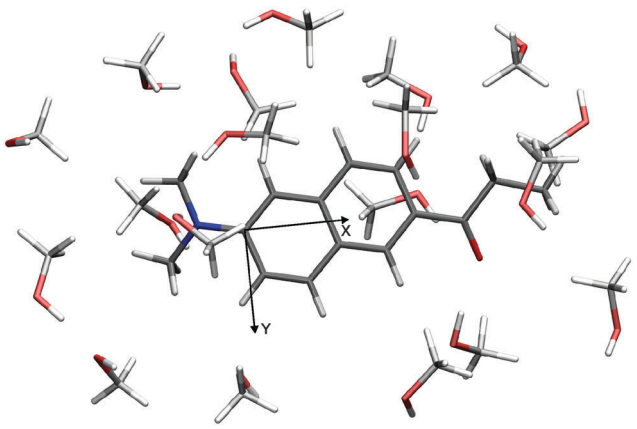

Fig. 1 Cluster system, consisting of PRODAN and MeOH within 3 Å, used in supermolecular QM calculations as well as in the PE and PE-EEF calculations, in which PRODAN constitutes the quantum region. In black: coordinate system of PRODAN used to define the angles in Table 2.

Table 2 Excitation energies ΔE_{01} (eV), oscillator strengths f, angles $\theta_{e_x}^{\mu_{01}}$ (degrees) between the transition dipole and the x-axis (see Fig. 1), and 2PA cross sections σ^{2PA} (1 GM = 10^{-50} cm^4 photon^{-1} s^{-1}), of the lowest singlet excited state of four PRODAN–MeOH clusters computed using the PE scheme with (PE-EEF) or without (PE) effective external field effects included as well as the corresponding full QM calculations

Configuration	Model	ΔE_{01}	$\theta_{e_x}^{\mu_{01}}$ [a]	f	σ^{2PA}
1 (19 MeOH)	vac	3.97	15.7	0.17	16
	PE	3.93	10.3	0.42	51
	PE-EEF		9.8	0.36	41
	QM	3.91	9.5	0.36	42
2 (15 MeOH)	vac	3.86	31.5	0.27	23
	PE	3.73	9.0	0.47	58
	PE-EEF		6.3	0.42	53
	QM	3.74	6.1	0.41	54
3 (18 MeOH)	vac	3.81	36.6	0.28	24
	PE	3.60	9.8	0.44	60
	PE-EEF		9.2	0.39	50
	QM	3.61	10.0	0.38	48
4 (19 MeOH)	vac	3.90	30.8	0.23	20
	PE	3.84	15.0	0.32	35
	PE-EEF		12.0	0.28	32
	QM	3.84	12.5	0.26	30

[a] The angle between $\boldsymbol{\mu}_{01}$ and the x-axis is the smallest of $\theta_{e_x}^{\mu_{01}}$ and $180^\circ - \theta_{e_x}^{\mu_{01}}$.

The effective external field corrected 1PA and 2PA properties based on four arbitrarily chosen MD configurations are compiled in Table 2, together with the standard values obtained by neglecting these effects. For comparison, we also include the results obtained for isolated PRODAN (vac), adopting the in-solution geometry from the corresponding cluster model.

The PE scheme reproduces well the excitation energies and absorption cross sections from the supermolecular calculations on solvated PRODAN. In particular, the effective external field corrected absorption cross sections are consistently much closer to the full QM results compared to those computed without these effects, validating the correctness of the formalism presented in this work. The average absolute errors are ~6% and 18% with and without effective external field corrections, respectively. While the PE-EEF oscillator strengths are systematically overestimated with respect to the full QM results, the picture is less clear for the 2PA cross sections. This can be expected, noting that (i) the effective external field contribution to the 2PA cross section in the supermolecular quadratic response treatment, in contrast to 1PA, does not translate into eqn (32), and (ii) the PE scheme neglects excitation channels in the environment that can serve as intermediate states, although the significantly larger energy spacing in MeOH effectively reduces such intermolecular contributions.

The computed results presented in Table 2 show that the inclusion of both the dynamic reaction field and the effective external field is needed for an accurate reproduction of the environment-mediated effects on 1PA and 2PA properties. Having established the performance of the effective external field corrected PE model with respect to supermolecular calculations on the solute–solvent test system, we proceed to investigate local field effects in a complex heterogeneous protein scaffold.

4.2 The red fluorescent protein DsRed

Since the discovery of the green fluorescent protein (GFP), fluorescent proteins (FPs) have become indispensable tools for noninvasive real-time bio-imaging.[80] The absorption and fluorescence colors of the lowest $\pi \rightarrow \pi^*$ transition are mainly controlled by the structure of the central chromophore. For instance, the spectra of the red fluorescent protein, DsRed, are red-shifted with respect to the GFP counterparts due to an acylimine elongation of the chromophore unit. In addition, and specifically relevant for selecting DsRed for this study, the optical properties may be substantially modulated by the local environment of the chromophore, as seen from the color and intensity variations across a series of red FPs that possess the same chromophore as DsRed.[11,81] In particular, the changes in 2PA cross sections have been correlated with variations in the local electric field furnished by the different proteins.[82] By applying the PE model, we recently demonstrated the importance of both the static and dynamic reaction field contributions to the local field on the tuning of the 1PA and 2PA properties of the lowest $\pi \rightarrow \pi^*$ transition in DsRed.[69] Based on this finding, it is interesting to also examine the implications of the remaining effective external field effects.

In Table 3, we present the 1PA and 2PA properties of the lowest $\pi \rightarrow \pi^*$ transition in the DsRed protein computed with and without effective external field effects, together with the corresponding results for the isolated DsRed chromophore (retaining the in-protein geometry). To distinguish the effects of the dynamic reaction field, we also provide the corresponding values obtained by excluding explicit polarization in the property calculations (labeled FPE for frozen PE), *i.e.*, where both dynamic reaction field and effective external field effects are disregarded. As reported in our previous work,[69] inclusion of the dynamic reaction field of the protein environment leads to an intensification of the 1PA and 2PA cross sections as well as a red-shifted excitation energy. Within a response framework, the pertinent quantity dictating these changes is the electrostatic potential produced by the environmental response to the first-order $\pi \rightarrow \pi^*$ transition electric field of the quantum region. Fig. 2 displays this potential on a surface of the DsRed chromophore, defined by the van der Waals atomic radii. As seen from the color gradient, the dipoles induced in the environment by the transition electric field exert an electric field across the conjugation pathway of the chromophore (*x*-direction, see Fig. 3), as expected from the underlying leading transition dipole term roughly being aligned with the *x*-axis (*cf.* transition dipole moments provided in Table 3). Taking effective external field effects into account not only counteracts the enhancement due to the dynamic reaction field but also reduces the absorption cross sections to a level below the one for the isolated chromophore.

For a (pseudo) one-dimensional dipolar chromophore, where the transition and difference dipole moments upon excitation are almost aligned, the local field factor effects on the 2PA cross section may be deduced (provided a non-dominating $\mathbf{E}^{[3]}$ contribution[84]) from the corresponding modifications of the 1PA cross section. Based on our previous analysis of the 1PA and 2PA

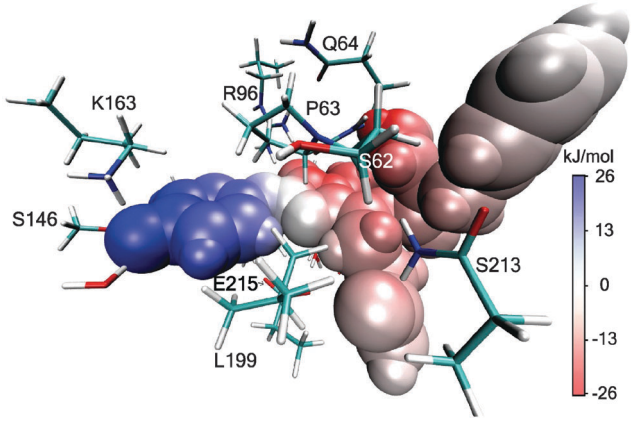

Fig. 2 Electrostatic potential (reported as energies resulting from the interaction with a unit point charge) produced by the induced dipoles in the environment due to the transition density of the lowest excited $\pi \rightarrow \pi^*$ state in DsRed. While the absolute directions of the dipoles induced by the transition electric field of the quantum region are arbitrary, their relative orientations are fixed. The selection of residues shown in wire representation corresponds to those defining the DsRed cluster model. The figure was prepared using VMD Molecular Graphics Viewer.[83]

Table 3 Excitation energies ΔE_{01} (eV), transition dipole moments $\boldsymbol{\mu}_{01}$ (a.u.), oscillator strengths *f*, and 2PA cross sections σ^{2PA} (GM) of the lowest singlet excited state of DsRed computed using the PE scheme with (PE-EEF) or without (PE) effective external field effects included. The Cartesian directions are given in Fig. 3

Model	ΔE_{01}	$\lvert\mu_{01}^x\rvert$	$\lvert\mu_{01}^y\rvert$	$\lvert\mu_{01}^z\rvert$	f	σ^{2PA}
vac[a]	2.53	4.12	1.27	0.42	1.16	47
DsRed protein						
FPE	2.97	3.89	0.89	0.31	1.17	60
PE	2.80	4.30	0.84	0.27	1.32	106
PE-EEF		3.13	0.61	0.04	0.70	30
DsRed cluster model (242 atoms)						
FPE	3.07	3.69	0.82	0.31	1.08	58
PE	2.96	3.83	0.75	0.28	1.11	77
PE-EEF		3.25	0.65	0.16	0.80	42
QM	2.92	3.36	0.68	0.19	0.84	38

[a] Vacuum results are taken from ref. 69 and correspond to the chromophore geometry enforced by the protein scaffold.

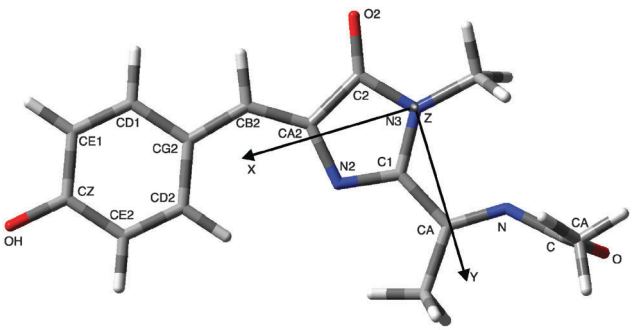

Fig. 3 Coordinate system defining Cartesian components of vector and tensor quantities as well as the atom labels adopted for the DsRed chromophore.

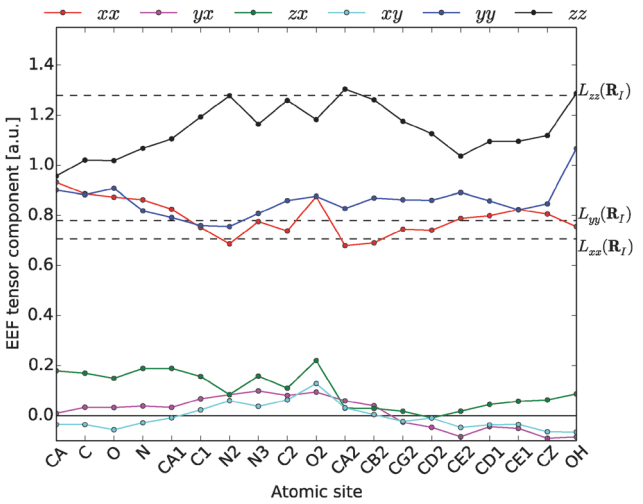

Fig. 4 Variations in the effective external field tensor across the heavy atoms in the conjugated pathway of the DsRed chromophore (see Fig. 3 for atom nomenclature). The horizontal lines indicate the diagonal elements of the effective external field tensor probed at the center, $\boldsymbol{R}_I$, of the imidazoline ring. The *ba* off-diagonal components behave similarly to the *ab* counterparts.

properties of DsRed,[69] the 2PA transition probability of the lowest excitation can be reasonably described within a one-dimensional (along *x*, *cf.* Fig. 3) two-state model. In line with this, we find, by comparing the 1PA and 2PA cross sections with and without effective external field effects, a 1.9- and 3.5-fold reduction of the oscillator strength and the 2PA cross section, respectively.

To validate the correctness of the effective external field effects on the lowest $\pi \rightarrow \pi^*$ transition obtained from the PE model, we further considered a cluster model (242 atoms), consisting of the chromophore and its nearest amino acids and biological water molecules (for details, see ESI of ref. 69), where full QM reference calculations are manageable. By comparing the resulting absorption cross sections to those obtained from the corresponding PE–DFT calculations with or without effective external field effects (lower part of Table 3), it is confirmed that the modulation of the field strength caused by the surrounding environment indeed diminishes the absorption cross sections, and that the inclusion of effective external field effects leads to values in better agreement with the full QM results.

As anticipated from the *x*-dominated transition properties, the field generated by the environment polarization induced by the external field screens the *x*-component of the electric field at the location of the chromophore. A direct quantification of the relation between the effective external field and the applied field is given by the effective external field tensor in eqn (19). Fig. 4 displays the components of the effective external field tensor evaluated at the position of the heavy atoms across the π-conjugated pathway in the DsRed chromophore. Indeed, the screening effects along the *x*- and also *y*-direction are reflected in corresponding diagonal elements of the effective external field tensor that are generally below unity. On the other hand, the *z*-component is mostly exceeding unity. For instance, at the center of the imidazoline ring (horizontal lines), the diagonal components of the effective external field tensor are $L_{xx}(\boldsymbol{R}_I)$ = 0.7, $L_{yy}(\boldsymbol{R}_I)$ = 0.8 and $L_{zz}(\boldsymbol{R}_I)$ = 1.3, respectively. This general amplification of the effective external field in the *z*-direction with respect to the external field hints that a *z*-allowed transition, in contrast to *x*- and/or *y*-dominated transitions, would be intensified by the effective external field effects. For comparison with the simplified spherical cavity picture in eqn (1), we recall that the Onsager cavity field factor gives $\sim$0.6 for n = 1.4. This clearly shows that the effective external field effects associated with a heterogeneous environment cannot be captured by a uniform scaling and that this more complex behavior should always be taken into account. Fig. 4 further displays the variations in the effective external field along the chromophore. Although the qualitative picture of the effective external field effect is almost consistent across the conjugation path, the tensor components vary significantly over the dimension of the molecule. This illustrates the limitations of using effective external field tensors, *i.e.*, the one-center truncated form in eqn (33), as a measure for the effective external field effects on response and transition properties.

5 Conclusions

We have presented a treatment of local field effects within the PE model that allows for the definition of the molecular and transition properties of molecules in solution as well as in more complex environments, reflecting the response to the externally applied field. Concretely, the model used in previous studies has been extended to account for the effective external field contribution to the local field so as to open the door for more direct comparisons to experimental measurements as well as full QM calculations. We have further introduced effective external field tensors, being the response of the effective external field to the applied field, to estimate the effects of this additional contribution and to draw an analogy to the simplified spherical cavity (Onsager) treatment. In this work, we focused on local field effects on the 1PA and 2PA properties of embedded molecules.

The applicability of the presented extension was demonstrated on PRODAN–methanol cluster models by comparing with the corresponding full QM reference calculations. Although the difference between the effective external field and the applied field is relatively small for this system, the account of such a difference consistently improves the comparison with the full QM reference. In addition, to examine the influence of local field effects in a heterogeneous environment we considered the 1PA and 2PA properties of the lowest $\pi \rightarrow \pi^*$ transition in the DsRed protein. In this case, the effective external field and dynamical reaction field contributions to the local field are found to act in opposite directions: the former more than counteracts the significant enhancement of the 1PA and 2PA cross-sections induced by the latter. In particular, we find the effective external field tensors to be strongly affected by the heterogeneity of the protein matrix. This means that the influence of the effective external field on

absorption properties depends critically on the orientation of the transition dipole moment of the excitation under study rather than being a uniform scaling for all transitions, as in the spherical cavity picture. This underlines the importance of a realistic description of both dynamical reaction field and effective external field contributions in the modeling of local field effects in heterogeneous environments.

Acknowledgements

The authors thank Maarten T. P. Beerepoot (University of Tromsø—The Arctic University of Norway) for useful comments. N. H. L. and J. K. acknowledge financial support from the Lundbeck Foundation and the Danish Council for Independent Research. J. K. acknowledges support from the Villum Foundation. Computations for the work described in this paper were supported by the DeIC National HPC Center, SDU.

References

1 S. D. Fried and S. G. Boxer, *Acc. Chem. Res.*, 2015, **48**, 998–1006.
2 B. H. Honig, W. L. Hubbell and R. F. Flewelling, *Annu. Rev. Biophys. Biophys. Chem.*, 1986, **15**, 163–193.
3 H. Nakamura, *Q. Rev. Biophys.*, 1996, **29**, 1–90.
4 S. D. Fried, S. Bagchi and S. G. Boxer, *Science*, 2014, **346**, 1510–1514.
5 J. Villa and A. Warshel, *J. Phys. Chem. B*, 2001, **105**, 7887–7907.
6 M. Štrajbl, A. Shurki, M. Kato and A. Warshel, *J. Am. Chem. Soc.*, 2003, **125**, 10228–10237.
7 A. Warshel, P. K. Sharma, M. Kato, Y. Xiang, H. Liu and M. H. M. Olsson, *Chem. Rev.*, 2006, **106**, 3210–3235.
8 S. Hammes-Schiffer, *Biochemistry*, 2013, **52**, 2012–2020.
9 C. T. Liu, J. P. Layfield, R. J. Stewart, J. B. French, P. Hanoian, J. B. Asbury, S. Hammes-Schiffer and S. J. Benkovic, *J. Am. Chem. Soc.*, 2014, **136**, 10349–10360.
10 J.-y. Hasegawa, K. J. Fujimoto and H. Nakatsuji, *ChemPhysChem*, 2011, **12**, 3106–3115.
11 M. Drobizhev, N. S. Makarov, S. E. Tillo, T. E. Hughes and A. Rebane, *Nat. Methods*, 2011, **8**, 393–399.
12 C. J. F. Bötcher and P. Bordewijk, *Theory of Electric Polarization*, Dielectrics in Static Fields, Elsevier, Amsterdam, 1973, vol. 1.
13 H.-A. Lorentz, *The Theory of Electrons and Its Applications to the Phenomena of Light and Radiant Heat*, Dover publications, 1952.
14 L. Onsager, *J. Am. Chem. Soc.*, 1936, **58**, 1486–1493.
15 R. Wortmann and D. M. Bishop, *J. Chem. Phys.*, 1998, **108**, 1001–1007.
16 D. R. Martin and D. V. Matyushov, *Europhys. Lett.*, 2008, **82**, 16003.
17 F. Terenziani, C. Katan, E. Badaeva, S. Tretiak and M. Blanchard-Desce, *Adv. Mater.*, 2008, **20**, 4641–4678.
18 E. Cancès, B. Mennucci and J. Tomasi, *J. Chem. Phys.*, 1997, **107**, 3032–3041.
19 J. Tomasi, B. Mennucci and R. Cammi, *Chem. Rev.*, 2005, **105**, 2999–3094.
20 R. Cammi, B. Mennucci and J. Tomasi, *J. Phys. Chem. A*, 1998, **102**, 870–875.
21 S. Pipolo, S. Corni and R. Cammi, *J. Chem. Phys.*, 2014, **140**, 164114.
22 R. Cammi, C. Cappelli, S. Corni and J. Tomasi, *J. Phys. Chem. A*, 2000, **104**, 9874–9879.
23 S. Corni, C. Cappelli, R. Cammi and J. Tomasi, *J. Phys. Chem. A*, 2001, **105**, 8310–8316.
24 C. Cappelli, S. Corni, B. Mennucci, R. Cammi and J. Tomasi, *J. Phys. Chem. A*, 2002, **106**, 12331–12339.
25 B. Mennucci, J. Tomasi, R. Cammi, J. R. Cheeseman, M. J. Frisch, F. J. Devlin, S. Gabriel and P. J. Stephens, *J. Phys. Chem. A*, 2002, **106**, 6102–6113.
26 C. Cappelli, A. Rizzo, B. Mennucci, J. Tomasi, R. Cammi, G. L. J. A. Rikken, R. Mathevet and C. Rizzo, *J. Chem. Phys.*, 2003, **118**, 10712–10724.
27 C. Cappelli, B. Mennucci, R. Cammi and A. Rizzo, *J. Phys. Chem. B*, 2005, **109**, 18706–18714.
28 M. Pecul, E. Lamparska, C. Cappelli, L. Frediani and K. Ruud, *J. Phys. Chem. A*, 2006, **110**, 2807–2815.
29 S. Pipolo, R. Cammi, A. Rizzo, C. Cappelli, B. Mennucci and J. Tomasi, *Int. J. Quantum Chem.*, 2011, **111**, 826–838.
30 C. Cappelli, F. Lipparini, J. Bloino and V. Barone, *J. Chem. Phys.*, 2011, **135**, 104505.
31 S. Pipolo, S. Corni and R. Cammi, *Comput. Theor. Chem.*, 2014, **1040**, 112–119.
32 R. Cammi, B. Mennucci and J. Tomasi, *J. Phys. Chem. A*, 2000, **104**, 4690–4698.
33 R. Cammi, L. Frediani, B. Mennucci and J. Tomasi, *THEOCHEM*, 2003, **633**, 209–216.
34 L. Ferrighi, L. Frediani, C. Cappelli, P. Sałek, H. Ågren, T. Helgaker and K. Ruud, *Chem. Phys. Lett.*, 2006, **425**, 267–272.
35 J. M. H. Olsen, K. Aidas and J. Kongsted, *J. Chem. Theory Comput.*, 2010, **6**, 3721–3734.
36 J. M. H. Olsen and J. Kongsted, *Adv. Quantum Chem.*, 2011, **61**, 107–143.
37 E. D. Hedegård, N. H. List, H. J. Aa. Jensen and J. Kongsted, *J. Chem. Phys.*, 2013, **139**, 044101.
38 L. Jensen, M. Swart and P. T. van Duijnen, *J. Chem. Phys.*, 2005, **122**, 034103.
39 K. Sneskov, T. Schwabe, J. Kongsted and O. Christiansen, *J. Chem. Phys.*, 2011, **134**, 104108.
40 N. H. List, M. T. P. Beerepoot, J. M. H. Olsen, B. Gao, K. Ruud, H. J. Aa. Jensen and J. Kongsted, *J. Chem. Phys.*, 2015, **142**, 034119.
41 X. S. Raymond, *Elementary Introduction to the Theory of Pseudo-differential Operators*, CRC Press, Boca Raton, Florida, 1991.
42 J. M. H. Olsen, PhD thesis, University of Southern Denmark, Odense, Denmark, 2012.
43 T. Helgaker, P. Jørgensen and J. Olsen, *Molecular Electronic-Structure Theory*, Wiley, 2000.
44 J. G. Ángyán, *J. Math. Chem.*, 1992, **10**, 93–137.
45 J. G. Ángyán, *Int. J. Quantum Chem.*, 1993, **47**, 469–483.
46 M. Orozco and F. J. Luque, *Chem. Phys. Lett.*, 1997, **265**, 473–480.

47 J. Applequist, J. R. Carl and K.-K. Fung, *J. Am. Chem. Soc.*, 1972, **94**, 2952–2960.
48 N. Davari, S. Haghdani, P.-O. Åstrand and G. C. Schatz, *RSC Adv.*, 2015, **5**, 31594–31605.
49 O. Christiansen, P. Jørgensen and C. Hättig, *Int. J. Quantum Chem.*, 1998, **68**, 1–52.
50 E. P. Wigner, *Math. Naturwiss. Anz. Ung. Akad. Wiss.*, 1935, **53**, 477.
51 J. Olsen and P. Jørgensen, *J. Chem. Phys.*, 1985, **82**, 3235–3264.
52 C. Hättig, O. Christiansen and P. Jørgensen, *J. Chem. Phys.*, 1998, **108**, 8331–8354.
53 M. V. Matz, A. F. Fradkov, Y. A. Labas, A. P. Savitsky, A. G. Zaraisky, M. L. Markelov and S. A. Lukyanov, *Nat. Biotechnol.*, 1999, **17**, 969–973.
54 P. J. Stephens, F. J. Devlin, C. F. Chabalowski and M. J. Frisch, *J. Phys. Chem.*, 1994, **98**, 11623–11627.
55 A. D. Becke, *J. Chem. Phys.*, 1993, **98**, 5648–5652.
56 S. H. Vosko, L. Wilk and M. Nusair, *Can. J. Phys.*, 1980, **58**, 1200–1211.
57 C. Lee, W. Yang and R. G. Parr, *Phys. Rev. B: Condens. Matter Mater. Phys.*, 1988, **37**, 785–789.
58 R. Krishnan, J. S. Binkley, R. Seeger and J. A. Pople, *J. Chem. Phys.*, 1980, **72**, 650–654.
59 T. Clark, J. Chandrasekhar, G. W. Spitznagel and P. V. R. Schleyer, *J. Comput. Chem.*, 1983, **4**, 294–301.
60 M. Freindorf, Y. Shao, T. R. Furlani and J. Kong, *J. Comput. Chem.*, 2005, **26**, 1270–1278.
61 W. D. Cornell, P. Cieplak, C. I. Bayly, I. R. Gould, K. M. Merz, D. M. Ferguson, D. C. Spellmeyer, T. Fox, J. W. Caldwell and P. A. Kollman, *J. Am. Chem. Soc.*, 1995, **117**, 5179–5197.
62 T. Yanai, D. P. Tew and N. C. Handy, *Chem. Phys. Lett.*, 2004, **393**, 51–57.
63 T. H. Dunning, *J. Chem. Phys.*, 1989, **90**, 1007–1023.
64 R. A. Kendall, T. H. Dunning Jr. and R. J. Harrison, *J. Chem. Phys.*, 1992, **96**, 6796–6806.
65 L. Gagliardi, R. Lindh and G. Karlström, *J. Chem. Phys.*, 2004, **121**, 4494–4500.
66 K. Aidas, C. Angeli, K. L. Bak, V. Bakken, R. Bast, L. Boman, O. Christiansen, R. Cimiraglia, S. Coriani, P. Dahle, E. K. Dalskov, U. Ekström, T. Enevoldsen, J. J. Eriksen, P. Ettenhuber, B. Fernández, L. Ferrighi, H. Fliegl, L. Frediani, K. Hald, A. Halkier, C. Hättig, H. Heiberg, T. Helgaker, A. C. Hennum, H. Hettema, E. Hjertenæs, S. Høst, I.-M. Høyvik, M. F. Iozzi, B. Jansik, H. J. A. Jensen, D. Jonsson, P. Jørgensen, J. Kauczor, S. Kirpekar, T. Kjærgaard, W. Klopper, S. Knecht, R. Kobayashi, H. Koch, J. Kongsted, A. Krapp, K. Kristensen, A. Ligabue, O. B. Lutnæs, J. I. Melo, K. V. Mikkelsen, R. H. Myhre, C. Neiss, C. B. Nielsen, P. Norman, J. Olsen, J. M. H. Olsen, A. Osted, M. J. Packer, F. Pawlowski, T. B. Pedersen, P. F. Provasi, S. Reine, Z. Rinkevicius, T. A. Ruden, K. Ruud, V. Rybkin, P. Sałek, C. C. M. Samson, A. S. de Merás, T. Saue, S. P. A. Sauer, B. Schimmelpfennig, K. Sneskov, A. H. Steindal, K. O. Sylvester-Hvid, P. R. Taylor, A. M. Teale, E. I. Tellgren, D. P. Tew, A. J. Thorvaldsen, L. Thøgersen, O. Vahtras, M. A. Watson, D. J. D. Wilson, M. Ziolkowski and H. Ågren, *Wiley Interdiscip. Rev.: Comput. Mol. Sci.*, 2014, **4**, 269–284.
67 Dalton, A Molecular Electronic Structure Program, Release DALTON2015.0 (2015), see http://daltonprogram.org/.
68 O. Vahtras, *LoProp for Dalton*, 2014, DOI: 10.5281/zenodo.13276.
69 N. H. List, J. M. H. Olsen, H. J. Aa. Jensen, A. H. Steindal and J. Kongsted, *J. Phys. Chem. Lett.*, 2012, **3**, 3513–3521.
70 J. L. Tubbs, J. A. Tainer and E. D. Getzoff, *Biochemistry*, 2005, **44**, 9833–9840.
71 P. C. Hariharan and J. A. Pople, *Theor. Chim. Acta*, 1973, **28**, 213–222.
72 M. M. Francl, W. J. Pietro, W. J. Hehre, S. J. Binkley, M. S. Gordon, D. J. DeFrees and J. A. Pople, *J. Chem. Phys.*, 1982, **77**, 3654–3665.
73 W. J. Hehre, R. Ditchfield and J. A. Pople, *J. Chem. Phys.*, 1972, **56**, 2257–2261.
74 J. M. H. Olsen, N. H. List, K. Kristensen and J. Kongsted, *J. Chem. Theory Comput.*, 2015, **11**, 1832–1842.
75 P. T. Van Duijnen and M. Swart, *J. Phys. Chem. A*, 1998, **102**, 2399–2407.
76 A. Dreuw and M. Head-Gordon, *J. Am. Chem. Soc.*, 2004, **126**, 4007–4016.
77 S. Jakobsen, K. Kristensen and F. Jensen, *J. Chem. Theory Comput.*, 2013, **9**, 3978–3985.
78 J. M. H. Olsen, *The Polarizable Embedding (PE) Library (Development Version)*, 2014.
79 M. T. P. Beerepoot, D. H. Friese, N. H. List, J. Kongsted and K. Ruud, *Phys. Chem. Chem. Phys.*, 2015, **17**, 19306–19314.
80 D. M. Chudakov, M. V. Matz, S. Lukyanov and K. A. Lukyanov, *Physiol. Rev.*, 2010, **90**, 1103–1163.
81 M. Drobizhev, S. Tillo, N. Makarov, T. Hughes and A. Rebane, *J. Phys. Chem. B*, 2009, **113**, 855–859.
82 M. Drobizhev, S. Tillo, N. S. Makarov, T. E. Hughes and A. Rebane, *J. Phys. Chem. B*, 2009, **113**, 12860–12864.
83 W. Humphrey, D. Dalke and K. Schulten, *J. Mol. Graphics*, 1996, **14**, 33–38.
84 N. H. List, R. Zaleśny, N. A. Murugan, J. Kongsted, W. Bartkowiak and H. Ågren, *J. Chem. Theory Comput.*, 2015, **11**, 4182–4188.

